Decoherence predictions in a superconducting quantum processor using the steepest-entropy-ascent quantum thermodynamics framework

J. A. Montañez-Barrera [1,*] Michael R. von Spakovsky [2,†] Cesar E. Damian Ascencio [1,‡] and Sergio Cano-Andrade [1,§]

[1] *Department of Mechanical Engineering, Universidad de Guanajuato, Salamanca, GTO 36885, Mexico*

[2] *Department of Mechanical Engineering, Virginia Tech, Blacksburg, Virginia 24061, USA*

(Received 15 March 2022; accepted 7 September 2022; published 22 September 2022)

The current stage of quantum computing technology, called noisy intermediate-scale quantum technology, is characterized by large errors that prohibit it from being used for real applications. In these devices, decoherence, one of the main sources of error, is generally modeled by Markovian master equations such as the Lindblad master equation. In this paper, the decoherence phenomena are addressed from the perspective of the steepest-entropy-ascent quantum thermodynamics framework in which the noise is in part seen as internal to the system. The framework is as well used to describe changes in the energy associated with environmental interactions. Three scenarios, an inversion recovery demonstration, a Ramsey demonstration, and a two-qubit entanglement-disentanglement demonstration, are used to demonstrate the applicability of this framework, which provides good results relative to the demonstrations and the Lindblad equation; it does so, however, from a different perspective as to the cause of the decoherence. These demonstrations are conducted on the IBM superconducting quantum device ibmq_bogota.

DOI: 10.1103/PhysRevA.106.032426

I. INTRODUCTION

Decoherence, which is perhaps one of the most critical aspects of quantum computation, is the loss of information that exists in the subsystems of a quantum device. It is typically viewed as resulting from environmental effects and random disturbances that affect the capacity of quantum systems to store information. Hence, the development of realistic quantum computers requires understanding, controlling, and/or correcting for decoherence.

The typical approach to modeling decoherence is to use linear Markovian quantum master equations (QMEs) of the Kossakowski-Lindblad-Gorini-Sudrashan type to represent the dynamics of system state evolution [1–3] and the loss of correlation. These QMEs assume that the system interacts with an environment and that the only relevant effect is that on the system. Nevertheless, the QMEs are still linear in nature and, thus, can at best only mimic the nonlinear dynamics that may be in play. Despite this fact, QMEs have shown good agreement with experimental data [4–6]. Even so, if the weak interactions needed for the QMEs equations are real, Nakatani and Ogawa [2] have shown that the Born-Markov approximation for obtaining evolution equations, i.e., QMEs, cannot be used for composite systems in the strong-coupling regime, no matter how short the reservoir correlation time.

An alternative approach results when, instead of assuming that the relevant irreversible effect on the system is due to an environment, quantum mechanics is complemented with the second law of thermodynamics represented by the steepest-entropy-ascent (SEA) principle. Such an approach assumes that the irreversible effect is fundamental to the system itself. This idea can be traced back to the work of Hatsopoulos and coworkers [7–11] and has matured over the last four decades and grown substantially in the last decade. A consequence of this work has been the construction of dynamical models based on the SEA principle that explain nonequilibrium phenomena at all levels of description, from the macroscopic to the microscopic (e.g., [12–35]).

With the advent of noisy intermediate-scale quantum (NISQ) devices [36], the study and simulation of noise in quantum devices have attracted great attention. Applications range from error mitigation techniques [37–39] to the simulation of quantum devices with real noise [40–42] to the simulation of quantum algorithms with decoherent error to understand how this noise affects NISQ algorithms in quantum machine learning models [43]. Recent work suggests that the steepest-entropy-ascent quantum thermodynamics (SEAQT) framework is suitable for modeling decoherence in quantum computation as is shown in [18] where SEAQT is used to show the interaction of a quantum cavity with a qubit and in [19] where it is used to predict the state evolution of a two-qubit system when a controlled-PHASE (CPHASE) gate is applied to a double quantum dot architecture. Both models are compared with demonstrations and show good predictive capabilities.

In the present paper, the loss of coherence in three different scenarios is evaluated through demonstrations. First, a qubit relaxation demonstration is implemented to determine how fast the system loses information due to the interaction with the environment. This phenomenon is measured in terms of the time T_1. Next, the dephasing on individual qubits using

*ja.montanezbarrera@ugto.mx
†vonspako@vt.edu
‡cesar.damian@ugto.mx
§sergio.cano@ugto.mx

the Ramsey demonstration is evaluated. This demonstration measures the loss of phase by a system through time, which is quantified with the time T_2^*. The last demonstration is a two-qubit cross-resonance (CR) interaction. Here, the loss of entanglement by a composite system is evaluated. To conduct this experiment, a two-qubit system in a Bell state $|\Phi\rangle$ is entangled and disentangled. The demonstrations are conducted on IBM's ibmq_bogota quantum device in qubits 0–4 for the T_1 and T_2^* demonstration and in qubits 0 and 1 for the entanglement demonstration. The demonstration results are compared with simulations using the SEAQT framework and the Lindblad approach.

The paper is organized as follows. In Secs. II A–II D different features of the SEAQT equation of motion are laid out and discussed, while Sec. II E presents the Lindblad-type quantum master equation used here. Section III then describes the demonstration setup of IBM's ibmq_bogota quantum device for each of the three demonstrations conducted. Section IV then provides the results of the demonstrations and the simulations and a discussion of the results. The paper then wraps up with a number of conclusions in Sec. V.

II. MATHEMATICAL MODEL

A. SEAQT framework

In the SEAQT framework, the dynamics of the density operator, $\hat{\rho}$, of a quantum system is governed by both a symplectic (unitary) and a dissipation (nonunitary) term. The former, the so-called von Neumann term of quantum mechanics, captures the reversible (i.e., linear) dynamics of state evolution, while the latter, which is based on the principle of SEA, captures the irreversible (i.e., nonlinear) dynamics. This principle states that at every instant of time the density operator evolves in the direction of maximal entropy increase such that the conservation constraints placed on the generators of the motion (e.g., the Hamiltonian and the identity operator) are satisfied. Note that the view of physical reality assumed here is one in which the nonlinear dynamics of state evolution resulting from the dephasing phenomenon are intrinsic to the system and not a consequence of interactions with an environment. This contrasts with the standard open quantum system framework (see Sec. II E) that forms the basis for the Lindblad equation of motion, which assumes that this phenomenon is the result of a continual cyclic buildup and loss of correlations between the system and environment. As pointed out in Sec. I, this assumption fails if the system-environment coupling is strong [2], a limitation which does not apply to the SEAQT framework. Of course, in the case of the relaxation phenomenon, the SEAQT framework also assumes a system-environment interaction since this phenomenon involves an exchange of energy between the system and environment. However, there is no limitation in the SEAQT framework on the strength of the coupling.

The SEAQT equation of motion for a general quantum system [44] is written as

$$\frac{d\hat{\rho}}{dt} = -\frac{i}{\hbar}[\hat{H}, \hat{\rho}] - \sum_J \left(\frac{1}{\tau_{D_J}} \hat{D}_J \otimes \hat{\rho}_{\bar{J}} \right) \tag{1}$$

where $\hat{H}$ and $\hat{\rho}$ are the Hamiltonian and the density operator, respectively, for a composite system. The $\hat{\rho}_J (J = 1, 2, \ldots)$ are the density operators for each individual qubit with $\hat{\rho}_J = \mathrm{Tr}_{\bar{J}}(\hat{\rho})$ and $\bar{J}$ indicating the direct product on the Hilbert space that does not contain the subsystem J. In addition, the $\tau_{D_J} (J = 1, 2, \ldots)$ are internal-relaxation parameters that are positive constants or positive functionals of the $\hat{\rho}_J$, while the $\hat{D}_J (J = 1, 2 \ldots)$ are the dissipation operators for each qubit. To assure positivity and hermiticity of the density operator, $\hat{\rho}$, the latter operators are written as

$$\hat{D}_J = \tfrac{1}{2}[\sqrt{\hat{\rho}_J}\tilde{D}_J + (\sqrt{\hat{\rho}_J}\tilde{D}_J)^\dagger] \tag{2}$$

where the symbol † signifies the adjoint and each $\tilde{D}_J$ for a two-qubit system is expressed as

$$\tilde{D}_J = \frac{\begin{vmatrix} \sqrt{\hat{\rho}_J}(\hat{B}\ln\hat{\rho})^J & \sqrt{\hat{\rho}_J}(\hat{I})^J & \sqrt{\hat{\rho}_J}(\hat{H})^J \\ (\hat{I}, \hat{B}\ln\hat{\rho})^J & (\hat{I}, \hat{I})^J & (\hat{I}, \hat{H})^J \\ (\hat{H}, \hat{B}\ln\hat{\rho})^J & (\hat{H}, \hat{I})^J & (\hat{H}, \hat{H})^J \end{vmatrix}}{\begin{vmatrix} (\hat{I}, \hat{I})^J & (\hat{I}, \hat{H})^J \\ (\hat{H}, \hat{I})^J & (\hat{H}, \hat{H})^J \end{vmatrix}}. \tag{3}$$

Here $(\cdot, \cdot)^J$ is the Hilbert-Schmidt inner product defined on Hilbert space $\mathcal{H}^J$ by $(\hat{F}, \hat{G})^J = \mathrm{Tr}_J(\hat{\rho}_J\{(\hat{F})^J, (\hat{G})^J\})$ with $J = A, B$, $(\hat{F})^A = \mathrm{Tr}_B[(\hat{I}_A \otimes \hat{\rho}_B)\hat{F}]$, and $(\hat{F})^B = \mathrm{Tr}_A[(\hat{\rho}_A \otimes \hat{I}_B)\hat{F}]$. In Eq. (3), $\hat{B}$ is the projector onto the range of ρ, i.e., the idempotent operator that results from summing up all of the eigenprojectors of $\hat{\rho}$ belonging to its nonzero eigenvalues.

Note that the first term to the right of the equal sign in Eq. (1), the so-called Hamiltonian term, moves the density or state operator, $\hat{\rho}$, in the direction of a unitary isentropic evolution. In contrast, the dissipation operator in Eq. (1) for a given qubit, $\hat{D}_J$, describes the spontaneous attraction of the qubit's density operator in the local direction of SEA. This direction is orthogonal to the direction of the unitary evolution and compatible with mean values of the non-Hamiltonian time invariants. In other words, this term pulls the density operator in the direction of the orthogonal projection of the gradient of the entropy functional, $-\mathrm{Tr}(\hat{\rho}_J \ln \hat{\rho}_J)$, onto the hyperplane of constant $\mathrm{Tr}(\hat{\rho}_J \hat{I}_J)$ and $\mathrm{Tr}(\hat{\rho}_J \hat{H}_J)$. This is, in effect, an implementation of the maximum entropy production principle in quantum theory. Furthermore, from a variational standpoint, identifying the SEA direction at each state $\hat{\rho}$ (i.e., at each instant of time) is accomplished by looking at all possible paths through $\hat{\rho}$, with each path characterized by a possible choice of $\hat{D}_J$. The path with the highest entropy generated in the interval dt is chosen. For more details, the reader is referred to [13–15].

B. Equation for a system interacting with a reservoir

One way to represent the interaction between a system J and a reservoir R consists of considering the degrees of freedom of both subsystems to be orthogonal [45]. This allows one to represent the Hilbert space of the two subsystems as $\mathcal{H} = \mathcal{H}_S \oplus \mathcal{H}_R$. In this framework, the eigenenergies of both subsystems are independent and unentangled. The

representation of the dissipative term for the system is

$$\tilde{D}_{JR} = -\sqrt{\hat{\rho}_J}\frac{\begin{vmatrix} -\hat{B}\ln\hat{\rho}_J & \hat{I}_J & \hat{0}_J & \hat{H}_J \\ \langle s\rangle_J & P_J & 0 & \langle e\rangle_J \\ \langle s\rangle_R & 0 & P_R & \langle e\rangle_R \\ \langle es\rangle_J + \langle es\rangle_J & \langle e\rangle_J & \langle e\rangle_R & \langle e^2\rangle_J + \langle e^2\rangle_R \end{vmatrix}}{\Gamma}. \tag{4}$$

Here the expected values for the system are $\langle s\rangle_J = -\mathrm{Tr}(\hat{\rho}_J \ln\hat{\rho}_J)$, $\langle e\rangle_J = \mathrm{Tr}(\hat{\rho}_J\hat{H}_J)$, and $\langle es\rangle_J = -\mathrm{Tr}(\hat{\rho}_J\hat{H}_J\ln\hat{\rho}_J)$. Also, $|\cdot|$ is a determinant and Γ is a Gram determinant. Expanding this last expression results in

$$\tilde{D}_{JR} = \sqrt{\hat{\rho}_J}\left(\hat{B}\ln\hat{\rho}_J - \frac{B_1}{\Gamma}\hat{I}_J - \frac{B_3}{\Gamma}\hat{H}_J\right) \tag{5}$$

where

$$B_1 = \begin{vmatrix} \langle s\rangle_J & 0 & \langle e\rangle_J \\ \langle s\rangle_R & P_R & \langle e\rangle_R \\ \langle es\rangle_J + \langle es\rangle_R & \langle e\rangle_R & \langle e^2\rangle_J + \langle e^2\rangle_R \end{vmatrix}, \tag{6}$$

$$B_3 = \begin{vmatrix} \langle s\rangle_J & P_J & 0 \\ \langle s\rangle_R & 0 & P_R \\ \langle es\rangle_J + \langle es\rangle_R & \langle e\rangle_J & \langle e\rangle_R \end{vmatrix}, \tag{7}$$

$$\Gamma = \begin{vmatrix} P_J & 0 & \langle e\rangle_J \\ 0 & P_R & \langle e\rangle_R \\ \langle e\rangle_J & \langle e\rangle_R & \langle e^2\rangle_J + \langle e^2\rangle_R \end{vmatrix}. \tag{8}$$

In the limit, when the number of eigenlevels of the reservoir P_R are much greater than those of the system P_J ($P_R \ll P_J$), one can show that B_3 reduces to

$$\frac{B_3}{\Gamma} \approx \frac{\langle es\rangle_R - \langle e\rangle_R\langle s\rangle_R}{\langle e^2\rangle_R - \langle e\rangle_R^2}. \tag{9}$$

Now assuming a canonical distribution for the reservoir characterized by the inverse temperature β_R and the Hamiltonian $\hat{H}_R$, B_3 is approximately

$$\frac{B_3}{\Gamma} \approx -\beta_R. \tag{10}$$

Therefore, $\tilde{D}_J$ of Eq. (3) for the system (i.e., for J) interacting with a reservoir can be expressed as

$$\tilde{D}_{JR} = \sqrt{\hat{\rho}_J}[\hat{B}\ln\hat{\rho}_J + \langle s\rangle_J\hat{I}_J + \beta_R(\hat{H}_J - \langle e\rangle_J\hat{I}_J)]. \tag{11}$$

The first two terms in Eq. (11) account for dephasing in the system, while the last term, i.e., $\beta_R(\hat{H}_J - \langle e\rangle_J\hat{I}_J)$, accounts for relaxation.

C. Model of relaxation and dephasing

Even though Eq. (11) by its own can represent the phenomena of relaxation and dephasing, experimental results show that those phenomena are happening at different rates. This can be taken into account by increasing or decreasing the value of β_R in Eq. (11) relative to the rate at which the relaxation occurs or, alternatively, by separating the effects of the phenomenon of relaxation from that of dephasing as in the Lindblad equation. Therefore, in the SEAQT framework, the phenomenon of dephasing is coupled with that of relaxation, and the general form of the SEAQT equation of motion, Eq. (1), is modified to include the effects of the reservoir interaction that only generates the relaxation transition, i.e., with $\beta_R(\hat{H}_S - \langle e\rangle_S\hat{I}_S)$ in Eq. (11). Therefore, the equation of motion for this case is written as

$$\frac{d\hat{\rho}}{dt} = -\frac{i}{\hbar}[\hat{H},\hat{\rho}] - \sum_J\left(\frac{1}{\tau_{D_J}}\hat{D}_J\otimes\hat{\rho}_{\bar{J}} + \frac{1}{\tau_{D_R}}\hat{D}_{JR}\otimes\hat{\rho}_{\bar{J}}\right) \tag{12}$$

where

$$\hat{D}_{JR} = \tfrac{1}{2}[\sqrt{\hat{\rho}_J}\tilde{D}_{JR} + (\sqrt{\hat{\rho}_J}\tilde{D}_{JR})^\dagger] \tag{13}$$

and

$$\tilde{D}_{JR} = \sqrt{\hat{\rho}_J}[\beta_R(\hat{H}_J - \langle e\rangle_J\hat{I}_J)]. \tag{14}$$

D. Qubit-reservoir interaction relaxation parameter

A usual approach for simulating a quantum process with the SEAQT equation of motion is to consider the relaxation parameter τ_D in Eq. (1) as a constant determined for a specific process. This approach has given good results when the process is at constant energy. However, the energy in the one-qubit demonstrations described in this paper changes considerably with time. A link between the rate of change of quantum states and the energy of the system proposed by Mandelstam and Tamm (see [46,47]) shows that the quantum speed limit can be bound by the energy of the system. In addition, Fermi's "golden rule" [48], which describes the transition rate between quantum states of a quantum system as a result of a weak perturbation, also describes such a transition in terms of the energy of the system. Thus, it is assumed here that the relaxation parameter fluctuates with the energy of the system. In particular, a qubit-reservoir relaxation parameter τ_{D_R} varying linearly with the expectation energy is assumed such that

$$\tau_{D_R}[\hat{\rho}(t)] = x_0(1 + \langle\hat{H}\rangle) \tag{15}$$

where x_0 is a constant to be determined. The Hamiltonian for a transmon qubit can be described using a Duffing oscillator [49] so that

$$\hat{H} = \omega\hat{b}^\dagger\hat{b} + \frac{\delta}{2}\hat{b}^\dagger\hat{b}(\hat{b}^\dagger\hat{b} - \hat{I}) \tag{16}$$

where ω and δ are the transmon frequency and anharmonicity, respectively, and $\hat{b}$ is the annihilation operator. Using the definitions that $\hat{b}^\dagger\hat{b} = \sum_j j|j\rangle\langle j|$ for the eigenlevels j of the transmon and $\omega_j = (\omega - \frac{\delta}{2})j + \frac{\delta}{2}j^2$, the Hamiltonian is rewritten as

$$\hat{H} = \sum_j \omega_j|j\rangle\langle j|. \tag{17}$$

For simplicity, it is assumed that the transmon is a two-level system. In that case, the Hamiltonian is given by

$$\hat{H} = -\tfrac{1}{2}\hbar\omega_q\hat{\sigma}_z \tag{18}$$

and, as a consequence, the relaxation parameter can be written as

$$\tau_{D_R}(\hat{\rho}) = x_0\{1 + \mathrm{Tr}[\hat{\rho}(t)\hat{\sigma}_z]\}. \tag{19}$$

Here, $\hat{\sigma}_z$ is the z-component Pauli matrix with the set of Pauli matrices given by $\hat{\sigma}_x = \left[\begin{smallmatrix}0 & 1\\ 1 & 0\end{smallmatrix}\right]$, $\hat{\sigma}_y = \left[\begin{smallmatrix}0 & -i\\ i & 0\end{smallmatrix}\right]$, and $\hat{\sigma}_z = \left[\begin{smallmatrix}1 & 0\\ 0 & -1\end{smallmatrix}\right]$.

E. Open quantum system model

The Lindblad equation, which is also known as the Gorini-Kossakowski-Sudarshan-Lindblad master equation, predicts the evolution of state of a quantum system as Markovian interactions between the system and multiple baths [1]. Generally, it uses a linear description to predict the nonlinear evolution of the density operator $\hat{\rho}$, preserving the laws of quantum mechanics and assuming a weak interaction between the system and the environment (baths). It has played an important role in quantum information and decoherence [50–53], which makes it suitable for the present paper. The equation of motion of the Lindblad type used here is expressed as

$$\frac{d\hat{\rho}_s}{dt} = -\frac{i}{\hbar}[\hat{H}, \hat{\rho}_s] + \frac{1}{2}\sum_{j=1}^{2}\gamma_j(2\hat{L}_j\hat{\rho}_s\hat{L}_j^\dagger - \hat{L}_j^\dagger\hat{L}_j\hat{\rho}_s - \hat{\rho}_s\hat{L}_j^\dagger\hat{L}_j) \tag{20}$$

where

$$\hat{L}_1 = \sqrt{\gamma_1}\hat{b} \tag{21}$$

and

$$L_2 = \sqrt{\gamma_2}\hat{\sigma}_z. \tag{22}$$

The L_1 operator is used to simulate the amplitude damping phenomenon (i.e., the relaxation), while the L_2 operator is employed to simulate dephasing. γ_1 is the strength of the relaxation and γ_2 is that of the dephasing.

III. DEMONSTRATION SETUP

The ibmq_bogota device used in the demonstrations is a superconducting quantum processor with a Falcon r4L architecture, five qubits, a quantum volume of 32, an average $T_1 = 88.34$ μs, an average $T_2 = 128.54$ μs, and an average controlled-NOT (CNOT) gate (see the Appendix) error of 1.056×10^{-2}. Qubits Q_0–Q_4 are employed with the following excitation frequencies: $f_{0,1,2,3,4} = 5.00, 4.85, 4.78, 4.86,$ and 4.98 GHz. Three demonstrations were conducted on this device: an inversion recovery demonstration, a Ramsey demonstration, and a two-qubit entanglement demonstration in the qubits 0 and 1. The first two demonstrations involved all of the qubits. The inversion recovery and the Ramsey demonstrations are based on the Hamiltonian given by

$$\hat{H} = \hbar\Delta\omega\hat{\sigma}_z + \hbar\theta_G(t)\hat{\sigma}_y \tag{23}$$

where $\Delta\omega = \omega_q - \omega_d$, ω_q, and ω_d are the qubit and electric-field frequencies, respectively, and $\theta_G(t)$ is the pulse applied to the qubit to generate a transition, a π rotation for the inversion recovery demonstration, and a $\pi/2$ rotation for the Ramsey demonstration.

For all three demonstrations, the number of shots, n, for each demonstration is 8192 and is the number of times that a demonstration is repeated to get back the probability of $\langle\hat{Z}\rangle = \mathrm{Tr}(\hat{\rho}\hat{\sigma}_z)$ on each qubit. The inversion recovery and the Ramsey demonstrations are repeated four times with some time lapse between each demonstration. Their variation is presented in the results with the points representing the mean value and the error bars the standard deviation. This number of shots is the maximum number allowed and reduces the statistical error of the demonstration to $1/\sqrt{n}$.

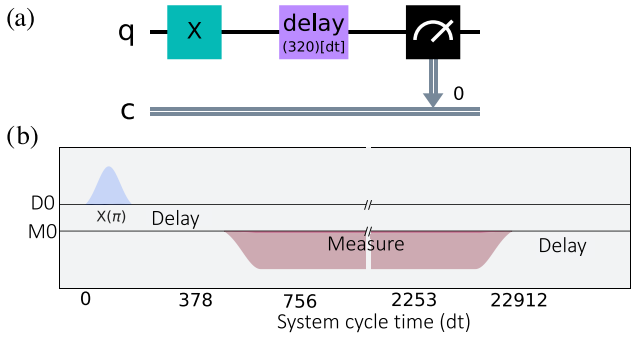

FIG. 1. Schematic representation of an inversion recovery demonstration characterized by T_1: (a) the pulse in the D_0 channel is a X_π gate, M_0 is the measurement, and (b) a pulse is applied in this channel to recover the state after the delay time. The demonstrations were conducted on the ibmq_bogota device from IBM, and using an open-pulse control in the QISKIT PYTHON library.

A. Inversion recovery

The inversion recovery demonstration provides information about how fast a qubit suffers thermalization because of its interaction with an environment (or reservoir). It is measured with the relaxation time T_1 where T_1 is the time that it takes the qubit to reach $1 - 1/e$ or 63% of its initial condition. Here, a π pulse gate (X gate) is used to move the system from state $|0\rangle$ to state $|1\rangle$. Next, a delay time is applied and measurement made. This process is repeated with 25 different delay times, ranging from 0 to 42.6 μs. What is observed is a decay of the probability of being in state $|1\rangle$. This decay can be approximated with the relation

$$\hat{\rho}(t) = \hat{\rho}(0)(1 - e^{-t/T_1}) \tag{24}$$

where $\hat{\rho}(0)$ is the density operator at time zero, t is the time, and T_1 is the relaxation time constant. Figure 1 schematically shows the circuit and the pulse representation of this demonstration. Here, D_0 is the channel, which transmits the signals to the qubits, allowing single-qubit gate operations, and M_0 is a measurement channel, which transmits a measurement stimulus pulse for readout. The pulse on D_0 is an X gate. This X_π gate's pulse is known as a derivative removal via an adiabatic gate (DRAG) [54] composed of a Gaussian shaped pulse $\theta_G(t) = \frac{1}{\sqrt{2\pi}\sigma}e^{-(\frac{t-t_0}{\sigma})^2}$ with rotation π about the y axis and a derivative of the Gaussian pulse responsible for eliminating X_π imperfections about the x axis. The X_π has a gate time of $t_g = 35.2$ ns where $\sigma = t_g/4$.

B. Ramsey demonstration

The Ramsey demonstration measures the dephasing time T_2^* and the qubit detuning [55]. Ideally, the frequency used for the pulse rotations is the resonant frequency of the qubit. However, due to imperfections and an inability to tune the resonant frequency, the qubit suffers from an oscillation proportional to the detuning. On the other hand, the dephasing phenomenon moves the qubit's Bloch vector towards the

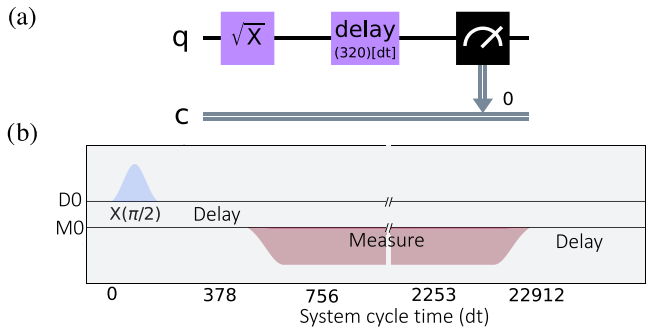

FIG. 2. Schematic representation of the Ramsey demonstration (a) circuit mode and (b) pulse mode to determine the coherence time T_2^*: The demonstration is conducted using the ibmq_bogota device and the pulse level control from IBMQ.

center of the Bloch sphere. The demonstration consists in applying a $X_{\pi/2}$ gate pulse on the drive channel D_0 and then allowing the system to evolve during a delay time, after which the qubit $\langle\hat{Z}\rangle$ observable is measured. Figure 2 presents the circuit and pulse representation for the demonstration to determine T_2^* relative to qubit zero.

C. Two-qubit entanglement state demonstration

The two-qubit entanglement state demonstration, shown in Fig. 3, consists of an entanglement and disentanglement scenario where the Bell state $|\Phi\rangle = 1/\sqrt{2}(|00\rangle + |11\rangle)$ is obtained in the case of maximum entanglement. This is achieved using a Hadamard gate on the control qubit followed by a CR protocol with a Han echo sequence on the CR channel [56,57]. This sequence is used to reduce the noise of the CR channel due to imperfections of the pulse applied. This is explained in detail in the Appendix. In Fig. 3, D_0 and D_1 are the drive channels for Q_0 and Q_1, respectively, and U_1 is the control channel for the interaction between Q_0 and Q_1. A modification of the default ibmq_bogota pulse calibration is used with a

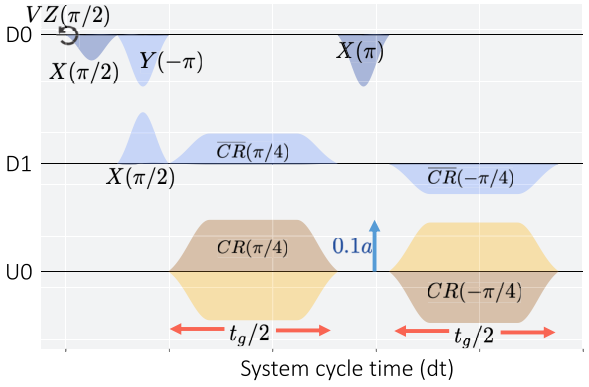

FIG. 3. The circuit to create the entanglement and disentanglement sequence: here, $t_g/2$ is the width of the CR pulse and 0.1a corresponds to the amplitude of the pulse where "a" is the default amplitude of the CR pulse for a CNOT gate. The channel D_0 represents the pulses on the control qubit, channel D_1 represents the pulses on the target qubit, and the brown and yellow pulses in U_1 represent the CR pulses that entangle both qubits.

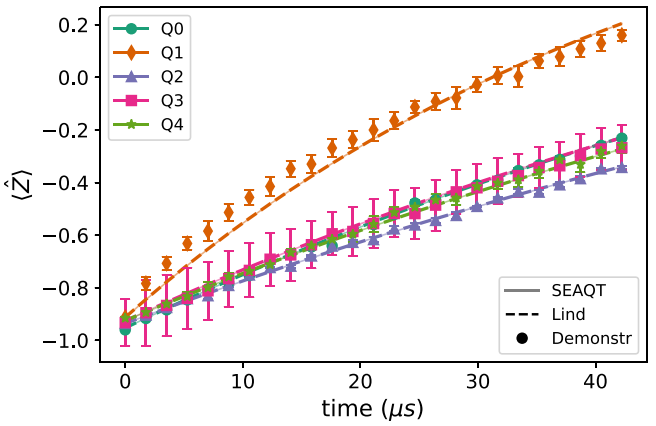

FIG. 4. Results from the inversion recovery demonstration for the time evolution of the $\langle\hat{Z}\rangle$ component or observable: The demonstration results for all five qubits are compared with simulation results from the SEAQT and the Lindblad equations of motion. The error bars represent the standard deviation.

change in the U_1 and D_0 amplitude to 0.1 of the default pulses during the CR section. In addition, the CR pulse width is modified from $t_g = 0$ to 20.45 μs with 30 intermediate pulse widths. Here, a maximum time of 20.45 μs, which is different from the time of the one-qubit demonstrations, is used because there is a limitation on the number of samples that can be created for a pulse in the IBM quantum hardware. In this case, that limit is closed to 20.45 μs for the CR pulse. Furthermore, for the one-qubit experiments, a delay time, which does not involve a sample pulse, is used. To construct the density state operator, a tomography process based on the work of Smolin *et al.* [58] is used with nine independent measurements to recover the two-qubit system density operator.

IV. RESULTS

A. Inversion recovery demonstration

The inversion recovery demonstration is used to characterize how fast a qubit loses information because of an interaction with the environment. Figure 4 shows the demonstration results of the $\langle\hat{Z}\rangle$ component for the five qubits of ibmq_bogota. As seen, the probability of getting state $|1\rangle$ monotonically decreases with time until it reaches a point close to the $|0\rangle$ state. This phenomenon is modeled using the Lindblad equation employing an annihilation operator in the master equation. To model this phenomenon within the SEAQT framework, the modification of its equation of motion outlined in Sec. II B is used. The results show that both the Lindblad and SEAQT models produce similar results for this demonstration. Models to fit the constants γ_1 and γ_2 for the Lindblad equation and τ_{D_R} for the SEAQT equation of motion are used.

The results seen in this figure indicate that the qubit that loses information the fastest is Q_1, while the loss for the other four qubits is significantly less. In addition, there is some deviation between the demonstrations and the Lindblad and SEAQT predictions. This deviation could come from either source of coherent errors or instabilities of near-resonant two-level systems coupled to the qubit. This phenomenon is

TABLE I. Summary of the simulation and parameter values used for each of the ibmq_bogota qubits.

Parameter	Q_0	Q_1	Q_2	Q_3	Q_4
$x_0(\tau_{D_R})$ (μs)	117.5	60.5	141.3	117.5	130.6
τ_{D_J} (μs)	40.6	11.3	43.9	28.1	49.8
$\tau_{D_J}^{2Q}$ (μs)	26.5	25.5			
$1/\gamma_1$ (μs)	184.3	97.25	231.5	190.2	206.13
$1/\gamma_2$ (μs)	751.4	73.2	637.6	277.4	692.1
T_1 (μs)	24.3	71.2	5.9	96.6	100.7
T_2 (μs)	41.9	41.9	59.1	160.5	171.1
Δf (kHz)	152.6	161.1	303.1	128.7	88.5

usually reported in these kind of devices [59]. The Lindblad relaxation and dephasing strength parameter values and the SEAQT qubit-reservoir $[x_0(\tau_{D_R})]$ and single-qubit dephasing parameter (τ_{D_J}) values used for each qubit are shown in Table I as are the characteristic relaxation and dephasing times found in the demonstration. The table also includes the detuning frequency, Δf, for each qubit. Note that the two-qubit dephasing parameter $\tau_{D_J}^{2Q}$ values are not used in this demonstration but instead in the second scenario of the two-qubit entanglement gate demonstration of Sec. IV C.

As shown in Eq. (19), the value of τ_{D_R} depends on the evolution of $\hat{\rho}$. As $\hat{\rho}$ approaches state $|0\rangle$, the relaxation parameter τ_{D_R} increases, which translates into a decrease in the dissipation experienced by the qubit-reservoir interaction. The evolution of τ_{D_R} for each qubit is shown in Fig. 5. As can be seen, the rate of increase of τ_{D_R} for Q_1 is significantly less than that for the other qubits and as a consequence the rate of information loss in Q_1 is in general greater than that for any of the other qubits as shown in Fig. 4.

B. Ramsey demonstration

Figure 6 shows results for the Ramsey demonstration of the time evolution of the $\langle\hat{X}\rangle$ component or observable. The oscillations observed in this demonstration are due to the detuning frequency Δf values given in Table I. As can be seen, the amplitude of the oscillation decays with increments in the delay time for all the qubits of the ibmq_bogota. This phenomenon, called *dephasing*, is responsible for the loss of

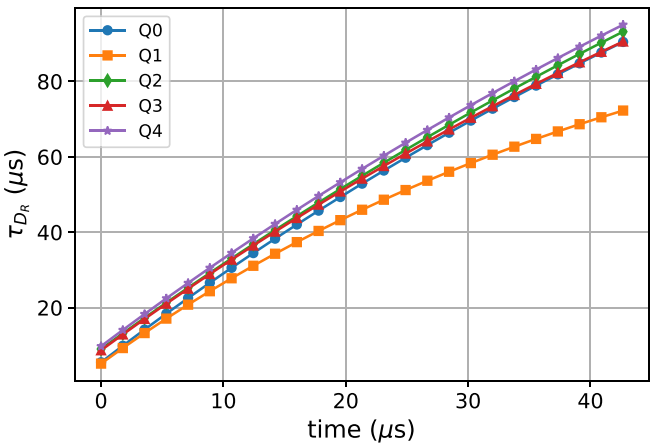

FIG. 5. Evolution in time of τ_{D_R} for each qubit.

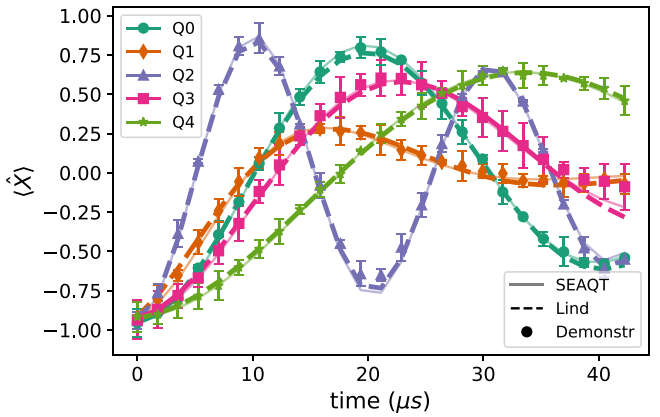

FIG. 6. Results from the Ramsey demonstration for the time evolution of the $\langle\hat{X}\rangle = \mathrm{Tr}(\hat{\rho}\hat{\sigma}_x)$ component: The demonstration results are compared with the simulation results of the SEAQT and Lindblad equations of motion for all five ibmq_bogota qubits. The error bars represent the standard deviation.

information of the $\langle\hat{X}\rangle$ and $\langle\hat{Y}\rangle$ observables of single qubits. The average rate of decay of dephasing is quantified by the T_2^* time, by τ_{DJ} for the case of the SEAQT equation of motion, and by $1/\gamma_2$ for the Lindblad equation. Values for these parameters are shown in Table I for the different qubits.

In addition to the decay of the $\langle\hat{X}\rangle$ observable seen in this demonstration, the relaxation phenomenon resulting from an interaction with the environment (reservoir) is present. The latter's effect on the $\langle\hat{Z}\rangle$ component or observable is shown in Fig. 7 and compared with the SEAQT and the Lindblad predictions. In this case, the values used for τ_{D_R} for the SEAQT equation of motion and γ_1 for the Lindblad equation are those obtained for the inversion recovery demonstration. As seen, predictions for both models agree quite well with the demonstration results.

C. Two-qubit entanglement-disentanglement demonstration

Finally, a two-qubit entanglement-disentanglement demonstration between the qubits Q_0 and Q_1 is executed to

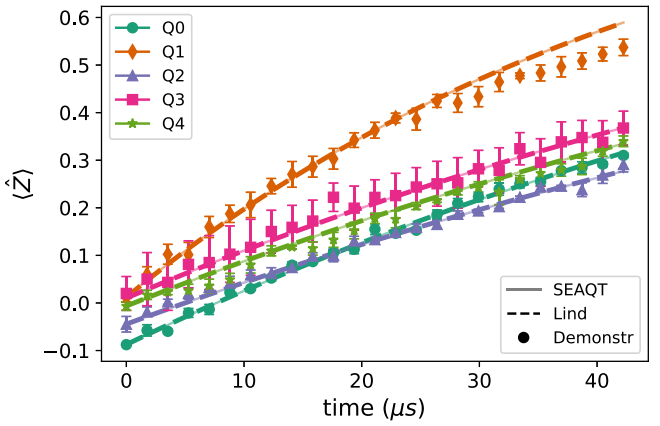

FIG. 7. Results from the Ramsey demonstration for the time evolution of the $\langle\hat{Z}\rangle$ component: The demonstration results are compared with simulation results of the SEAQT and Lindblad equation of motion for all five ibmq_bogota qubits. The error bars represent the standard deviation.

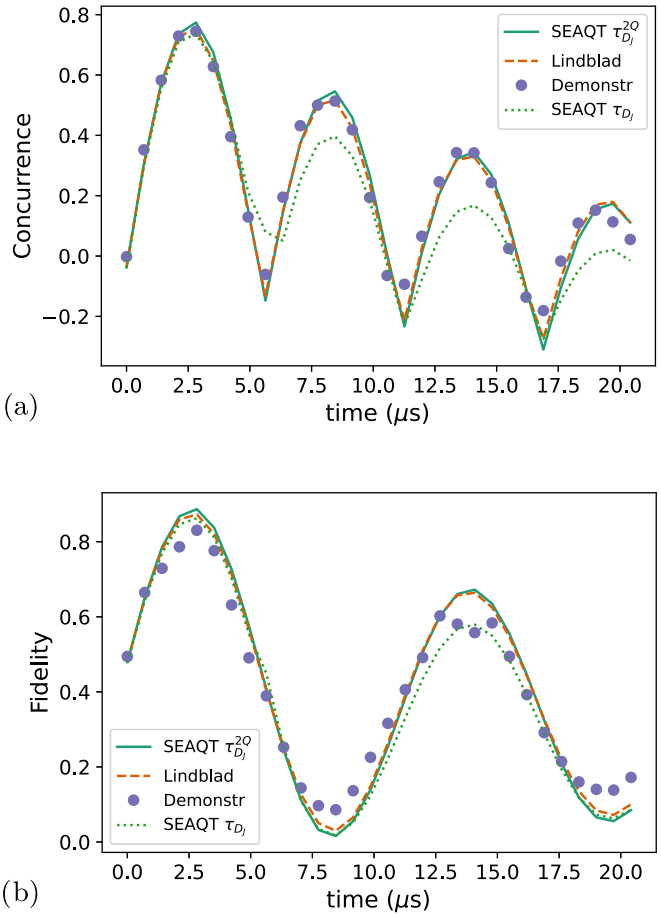

FIG. 8. Demonstration and model results for the two-qubit entanglement-disentanglement demonstration showing the time evolution of (a) the concurrence and (b) the fidelity.

explore the decay rate of information stored in the two-qubit system. This demonstration shows how the maximum entanglement is lost with time. The results in Fig. 8(a) show a continuous loss in the maximum concurrence as the width of the CR sequence goes from 0 to 20.45 μs. In an ideal case, the concurrence should be oscillating between 0 and 1. However, the maximum concurrence never reaches 1 and gradually decreases from a maximum value of about 0.75 to about 0.19 as the width of the CR pulse increases. The same is true for the fidelity shown in Fig. 8(b) in which the maximum fidelity decreases from about 0.85 to about 0.68 for the second peak.

Two different scenarios are tested with the SEAQT equation of motion. The first uses the relaxation τ_{D_R} and dephasing τ_{DJ} parameter values found for the single-qubit demonstrations with qubits Q_0 and Q_1, while the second keeps the relaxation parameter τ_{D_R} values of the single-qubit demonstrations but utilizes values for the dephasing parameters τ_{DJ}^{2Q} found from the present two-qubit demonstration. The results for the first scenario show that the decoherence is greater than what is found in the two-qubit demonstration (see the dotted-green line in Fig. 8). In contrast, the second case, which utilizes two-qubit demonstration dephasing values for $\tau_{D_J}^{2Q}$ and single-qubit demonstration qubit-reservoir values for τ_{D_R}, predicts the demonstration concurrence and fidelity values quite well as seen in Fig. 8 with the red-solid line. Here, the improved fit for scenario 2 is explained by the fact that the the T_1 relaxation and T_2^* dephasing times characterizing the demonstrations change with time, a conclusion supported by Burnett *et al.* [59], who indicate that the decay times for relaxation and dephasing are not constant but vary with time. In this scenario, demonstrations for dephasing and relaxation were conducted on the same day, while the two-qubit demonstration was taken some days later. This could influence the different decay rates. Another plausible explanation is that the disentanglement-entanglement demonstration is improving the decay rate of the decoherence phenomena by the dynamics involved. Further investigation with respect to this is needed but is beyond the scope of the present paper.

V. CONCLUSIONS

In this paper, an approach based on the principle of steepest entropy ascent is used to predict the relaxation, dephasing, and loss of entanglement phenomena in superconducting qubits during the state evolution of inversion recovery, Ramsey, and entanglement-disentanglement demonstrations. The results obtained suggest that the SEAQT framework can predict the different decoherence scenarios occurring in superconducting qubits. These results supplement the purely dephasing results found previously by applying the SEAQT framework to a CPHASE gate on a double-quantum-dot qubit device [19]. In the present paper, the phenomenon of relaxation, which requires an interaction with the environment and which was not previously addressed, is successfully modeled. The SEAQT framework is, thus, able to effectively describe both types of phenomena. Predictions of the effects of the relaxation and dephasing phenomena have been shown to be useful in mitigating errors in NISQ devices [60]. Thus, the SEAQT framework could potentially be used as the basis for an error mitigation scheme in such devices. The method to do so would be similar to the zero-noise extrapolation technique [37], but in this case different delay times would be used to make the extrapolation of a zero delay time such that the dephasing and relaxation noise is reduced. However, a comparison with the commonly used Lindblad equation would still be needed to determine the advantages and disadvantages of such an error mitigation technique.

Another point to make is that the use of a variable τ_{D_R} that depends on the energy of the system provides a relaxation parameter for the SEAQT equation of motion that results in predictions that compare well with the data for the relaxation and Ramsey demonstrations.

Clearly, the SEAQT framework is a reasonable model for predicting the dynamics of quantum protocols, providing an alternative approach for determining T_1 and T_2 in superconducting quantum processors. As described at the beginning of Sec. II A, conceptually the SEAQT framework treats the dephasing phenomenon as intrinsic to the system, while the open quantum system framework, which is the basis for the Lindblad equation, treats it extrinsically, requiring two limiting assumptions: weak couplings with an environment and a linear description of the nonlinear evolution of the density operator. Neither of these limitations applies to the SEAQT framework. Of course, with this loss of generality,

the computational cost of the Lindblad equation is less than that of the SEAQT equation but only slightly so. Furthermore, the SEAQT framework's greater generality results in an easier setup since the specific form of the environmental interaction needed by the Lindblad equation for the dephasing phenomenon is not required by the SEAQT equation, which treats this phenomenon intrinsically via the SEA principle. Even for the relaxation phenomenon, a specific form of the interaction is not needed by the SEAQT equation of motion. Of course, both the Lindblad and SEAQT equations of motion can be scaled to larger qubit arrays and do so on the basis of 2^N where N is the number of qubits in the array. Thus, since both equations are first-order ordinary differential equations in time, an array of up to at least 20 qubits could be run on a desktop computer (e.g., an iMac). Larger arrays would require additional computational resources although even then both approaches would in the end be limited to relatively small quantum devices or subsets of larger devices.

Additional detailed comparisons of the Lindblad and SEAQT approaches in predicting the behavior of one or more quantum devices are needed. Although the comparisons made here show little difference, past comparisons of SEAQT predictions with those developed by standard approaches found in the literature (e.g., Lindblad [19] and the correlation signal [18]) do show differences. For example, in [19], the loss of entanglement of a CPHASE gate in a singlet-triplet qubit implemented via confining two electrons to a double quantum dot in a two-dimensional electron gas positioned below a GaAs-AlGaAs heterostructure surface [61] is modeled. SEAQT predictions generally do as well as and at times better than those of the Lindblad approach. In [18], the SEAQT predictions of the time-dependent decoherence of the "meter" in a quantum measurement of a cavity quantum electrodynamic experiment are generally better and more physically realistic than those of the correlation signal [62] used by Brune *et al*. [63]. Though none of this is conclusive, it does suggest that the SEAQT framework is a viable alternative to existing approaches.

Finally, the possibility of conducting demonstrations on cloud-based quantum devices opens opportunities for testing different equations of motion and scenarios for the nonequilibrium evolution of quantum systems. Future work will focus on developing ways to mitigate the error inherent to these devices and recover as much of the information as possible that is lost in the operation of these devices.

ACKNOWLEDGMENTS

J.A.M.-B. thanks the National Council of Science and Technology (CONACyT), Mexico, for Grant No. CVU-736083. S.C.-A. and C.E.D.-A. gratefully acknowledge the financial support of CONACyT, Mexico, under its SNI program.. The authors acknowledge the use of IBM's Quantum services for this work.

APPENDIX

For the case of superconducting qubits as in the case of the IBM ibmq_bogota device, the CNOT gate is composed of a CR interaction [64] and single-qubit DRAG pulses with virtual z rotations [65,66]. In a recent paper, Magesan and Gambetta [67] introduced the effective Hamiltonian of a CR interaction, i.e.,

$$\hat{H}(\Omega) = \nu_{ZX}\frac{\hat{Z}\hat{X}}{2} + \nu_{IZ}\frac{\hat{I}\hat{Z}}{2} + \nu_{IX}\frac{\hat{I}\hat{X}}{2} + \nu_{ZI}\frac{\hat{Z}\hat{I}}{2} + \nu_{ZZ}\frac{\hat{Z}\hat{Z}}{2}, \tag{A1}$$

where $\{\hat{I}, \hat{X}, \hat{Y}, \hat{Z}\}$ are the identity and Pauli matrices. For the different tensor products (e.g., $\hat{Z}\hat{X}$), the convention is that the first acts on the control qubit and the second acts on the target qubit. The coefficients ν_{ij} in Eq. (A1) are functions of the system parameters and the CR pulse amplitude Ω. In this Hamiltonian, only the $\hat{Z}\hat{X}$ term, which is locally the equivalent of a CNOT gate, is of interest here. Applying the echo sequence $\hat{U} = \hat{X}\hat{I}\cdot e^{-i\hat{H}(-\Omega)t_g}\cdot\hat{X}\hat{I}\cdot e^{-i\hat{H}(\Omega)t_g}$, which as shown in Sundaresan *et al.* [68] can be modeled by $\hat{U} = A_{II}\hat{I}\hat{I} + A_{IY}\hat{I}\hat{Y} + A_{IZ}\hat{I}\hat{Z} + A_{ZX}\hat{Z}\hat{X}$, the following Hamiltonian is obtained:

$$\hat{H}_{\text{eff}} = \tilde{\nu}_{ZX}\frac{\hat{Z}\hat{X}}{2} + \tilde{\nu}_{IY}\frac{\hat{I}\hat{Y}}{2} + \tilde{\nu}_{IZ}\frac{\hat{I}\hat{Z}}{2}. \tag{A2}$$

Here, the $\tilde{\nu}_{i,j}$ are coefficients of the echo sequence effective Hamiltonian and the $\{A_{II}, A_{IY}, A_{IZ}, A_{ZX}\}$ are functions of these coefficients. If there is crosstalk or phase misalignment, the additional rotations $\hat{Z}\hat{Y}$ and $\hat{Z}\hat{Z}$ show up in Eq. (A2).

Two main strategies have been used to reduce the coherent error for the CR pulse, namely, an active cancellation on the target qubit [57] and the addition of target rotary pulses [68]. These strategies reduce the error in the two-qubit subspace and even on spectator qubits, which are neighbors of the target qubit, using the approach of Sundaresan *et al.* [68]. Both papers have a clear strategy for reducing coherent errors. First, they identify the unwanted CR Hamiltonian error terms remaining after the standard echo sequence. Second, they devise strategies to measure the error. Finally, they mitigate the error with additional pulses on the target qubit.

Our approach is to use this calibration process for the IBM ibmq_bogota device, creating an entanglement state for different coupling factors in ν_{ZX}.

[1] G. Lindblad, On the generators of quantum dynamical semigroups, Commun. Math. Phys. **48**, 119 (1976).

[2] M. Nakatani and T. Ogawa, Quantum master equations for composite systems: Is Born-Markov approximation really valid? J. Phys. Soc. Jpn. **79**, 084401 (2010).

[3] C. H. Chou, T. Yu, and B. L. Hu, Exact master equation and quantum decoherence of two coupled harmonic oscillators in a general environment, Phys. Rev. E **77**, 011112 (2008).

[4] Q. A. Turchette, C. J. Myatt, B. E. King, C. A. Sackett, D. Kielpinski, W. M. Itano, C. Monroe, and D. J. Wineland, Decoherence and decay of motional quantum states of a trapped atom coupled to engineered reservoirs, Phys. Rev. A **62**, 053807 (2000).

[5] B. A. Stickler, F. T. Ghahramani, and K. Hornberger, Rotational Alignment Decay and Decoherence of Molecular Superrotors, Phys. Rev. Lett. **121**, 243402 (2018).

[6] E. Barnes, Ł. Cywiński, and S. Das Sarma, Nonperturbative Master Equation Solution of Central Spin Dephasing Dynamics, Phys. Rev. Lett. **109**, 140403 (2012).

[7] G. N. Hatsopoulos and E. P. Gyftopoulos, A unified quantum theory of mechanics and thermodynamics. Part III. Irreducible quantal dispersions, Found. Phys. **6**, 561 (1976).

[8] G. N. Hatsopoulos and E. P. Gyftopoulos, A unified quantum theory of mechanics and thermodynamics. Part IIb. Stable equilibrium states, Found. Phys. **6**, 439 (1976).

[9] G. N. Hatsopoulos and E. P. Gyftopoulos, A unified quantum theory of mechanics and thermodynamics. Part IIa. Available energy, Found. Phys. **6**, 127 (1976).

[10] G. N. Hatsopoulos and E. P. Gyftopoulos, A unified quantum theory of mechanics and thermodynamics. Part I. Postulates, Found. Phys. **6**, 15 (1976).

[11] G. P. Beretta, J. Park, and G. N. Hatsopoulos, Quantum thermodynamics. A new equation of motion for a single constituent of matter, IL Nuovo Cimento **82**, 169 (1984).

[12] G. P. Beretta, Nonlinear model dynamics for closed-system, constrained, maximal-entropy-generation relaxation by energy redistribution, Phys. Rev. E **73**, 026113 (2006).

[13] G. P. Beretta, Steepest entropy ascent model for far-nonequilibrium thermodynamics: Unified implementation of the maximum entropy production principle, Phys. Rev. E **90**, 042113 (2014).

[14] G. P. Beretta, Nonlinear quantum evolution equations to model irreversible adiabatic relaxation with maximal entropy production and other nonunitary processes, Rep. Math. Phys. **64**, 139 (2009).

[15] G. P. Beretta, Maximum entropy production rate in quantum thermodynamics, J. Phys.: Conf. Ser. **237**, 012004 (2010).

[16] M. R. von Spakovsky and J. Gemmer, Some trends in quantum thermodynamics, Entropy **16**, 3434 (2014).

[17] A. Montefusco, F. Consonni, and G. P. Beretta, Essential equivalence of the general equation for the nonequilibrium reversible-irreversible coupling (GENERIC) and steepest-entropy-ascent models of dissipation for nonequilibrium thermodynamics, Phys. Rev. E **91**, 042138 (2015).

[18] S. Cano-Andrade, G. P. Beretta, and M. R. von Spakovsky, Steepest-entropy-ascent quantum thermodynamic modeling of decoherence in two different microscopic composite systems, Phys. Rev. A **91**, 013848 (2015).

[19] J. A. Montanez-Barrera, C. E. Damian-ascencio, M. R. von Spakovsky, and S. Cano-andrade, Loss-of-entanglement prediction of a controlled-PHASE gate in the framework of steepest-entropy-ascent quantum thermodynamics, Phys. Rev. A **101**, 052336 (2020).

[20] G. Li, M. R. von Spakovsky, and C. Hin, Steepest entropy ascent quantum thermodynamic model of electron and phonon transport, Phys. Rev. B **97**, 024308 (2018).

[21] G. Li, M. R. von Spakovsky, F. Shen, and K. Lu, Multiscale Transient and Steady-State Study of the Influence of Microstructure Degradation and Chromium Oxide Poisoning on Solid Oxide Fuel Cell Cathode Performance, J. Non-Equilib. Thermodyn. **43**, 21 (2017).

[22] G. Li and M. R. von Spakovsky, Steepest-entropy-ascent quantum thermodynamic modeling of the relaxation process of isolated chemically reactive systems using density of states and the concept of hypoequilibrium state, Phys. Rev. E **93**, 012137 (2016).

[23] G. Li and M. R. von Spakovsky, Study of the transient behavior and microstructure degradation of a SOFC cathode using an oxygen reduction model based on steepest-entropy-ascent quantum thermodynamics, in *Proceedings of the ASME 2015 International Mechanical Engineering Congress and Exposition*, Vol. 6B Energy (ASME, Houston, Texas, USA, 2015).

[24] G. Li, O. Al-Abbasi, and M. R. von Spakovsky, Atomistic-level non-equilibrium model for chemically reactive systems based on steepest-entropy-ascent quantum thermodynamics, J. Phys.: Conf. Ser. **538**, 012013 (2014).

[25] A. Kusaba, G. Li, M. R. von Spakovsky, Y. Kangawa, and K. Kakimoto, Modeling the non-equilibrium process of the chemical adsorption of ammonia on GaN(0001) reconstructed surfaces based on steepest-entropy-ascent quantum thermodynamics, Materials **10**, 948 (2017).

[26] A. Kusaba, G. Li, P. Kempisty, M. R. von Spakovsky, and Y. Kangawa, CH_4 adsorption probability on GaN(0001) and (000-1) during metalorganic vapor phase epitaxy and its relationship to carbon contamination in the films, Materials **16**, 972 (2019).

[27] R. Yamada, M. R. von Spakovsky, and W. T. Reynolds, Jr., A method for predicting nonequilibrium thermal expansion using steepest-entropy-ascent quantum thermodynamics, J. Phys.: Condens. Matter **30**, 325901 (2018).

[28] R. Yamada, M. R. von Spakovsky, and W. T. Reynolds, Predicting continuous and discontinuous phase decompositions using steepest-entropy-ascent quantum thermodynamics, Phys. Rev. E **99**, 052121 (2019).

[29] R. Yamada, M. R. von Spakovsky, and W. T. Reynolds, Jr., Low-temperature atomistic spin relaxation and non-equilibrium intensive properties using steepest-entropy-ascent quantum-inspired thermodynamics modeling, J. Phys.: Condens. Matter **31**, 505901 (2019).

[30] R. Yamada, M. R. von Spakovsky, and W. T. Reynolds Jr., Methodology of an application of the steepest-entropy-ascent quantum thermodynamic framework to physical phenomena in materials science, Comput. Mater. Sci. **166**, 251 (2019).

[31] R. Yamada, M. R. von Spakovsky, and W. T. Reynolds Jr., Kinetic pathways of ordering and phase separation using classical solid state models within the steepest-entropy-ascent quantum thermodynamic framework, Acta Mater. **182**, 87 (2020).

[32] I. Goswami, R. Bielitz, S. S. Verbridge, and M. R. von Spakovsky, A thermodynamic scaling law for electrically perturbed lipid membranes: Validation with steepest entropy ascent framework, Bioelectrochemistry **140**, 107800 (2021).

[33] J. McDonald, M. R. von Spakovsky, and W. T. Reynolds, Entropy-driven microstructure evolution calculated with the steepest-entropy-ascent quantum thermodynamic framework, arXiv:2108.11924 (2021).

[34] J. A. Montanez-Barrera, R. T. Holladay, G. P. Beretta, and M. R. von Spakovsky, Method for generating randomly perturbed density operators subject to different sets of constraints, arXiv:2112.12247.

[35] C. E. Smith and M. R. von Spakovsky, Comparison of the non-equilibrium predictions of Intrinsic Quantum Thermodynamics at the atomistic level with experimental evidence, J. Phys.: Conf. Ser. **380**, 012015 (2012).

[36] J. Preskill, Quantum computing in the NISQ era and beyond, Quantum **2**, 79 (2018).
[37] A. Kandala, K. Temme, A. D. Córcoles, A. Mezzacapo, J. M. Chow, and J. M. Gambetta, Error mitigation extends the computational reach of a noisy quantum processor, Nature (London) **567**, 491 (2019).
[38] R. Sagastizabal, X. Bonet-Monroig, M. Singh, M. A. Rol, C. C. Bultink, X. Fu, C. H. Price, V. P. Ostroukh, N. Muthusubramanian, A. Bruno, M. Beekman, N. Haider, T. E. O'Brien, and L. Dicarlo, Experimental error mitigation via symmetry verification in a variational quantum eigensolver, Phys. Rev. A **100**, 010302(R) (2019).
[39] K. N. Smith, G. S. Ravi, P. Murali, J. M. Baker, N. Earnest, A. Javadi-Abhari, and F. T. Chong, Error mitigation in quantum computers through instruction scheduling, arXiv:2105.01760
[40] P. Murali, J. M. Baker, A. J. Abhari, F. T. Chong, and M. Martonosi, Noise-adaptive compiler mappings for noisy intermediate-scale quantum computers, International Conference on Architectural Support for Programming Languages and Operating Systems—ASPLOS, arXiv:1901.11054 (2019).
[41] K. Noh, L. Jiang, and B. Fefferman, Efficient classical simulation of noisy random quantum circuits in one dimension, Quantum **4**, 318 (2020).
[42] M. L. Dahlhauser and T. S. Humble, Modeling noisy quantum circuits using experimental characterization, Phys. Rev. A **103**, 042603 (2021).
[43] S. Wang, E. Fontana, M. Cerezo, K. Sharma, A. Sone, L. Cincio, and P. J. Coles, Noise-induced barren plateaus in variational quantum algorithms, Nat. Commun. **12**, 6961 (2021).
[44] G. P. Beretta, E. P. Gyftopoulos, and J. L. Park, Quantum thermodynamics. A new equation of motion for a general quantum system, Il Nuovo Cimento **87**, 77 (1985).
[45] R. T. Holladay, Steepest-entropy-ascent quantum thermodynamic modeling of quantum information and quantum computing systems, Ph.D. thesis, Virginia Tech, 2019.
[46] L. Mandelstam and I. Tamm, The uncertainty relation between energy and time in a non-relativistic Quantum Mechanics, J. Phys. **9**, 249 (1945).
[47] A. del Campo, I. L. Egusquiza, M. B. Plenio, and S. F. Huelga, Quantum Speed Limits in Open System Dynamics, Phys. Rev. Lett. **110**, 050403 (2013).
[48] D. Braak and J. Mannhart, Fermi's Golden Rule and the Second Law of Thermodynamics, Found. Phys. **50**, 1509 (2020).
[49] B. Khani, J. M. Gambetta, F. Motzoi, and F. K. Wilhelm, Optimal generation of Fock states in a weakly nonlinear oscillator, Phys. Scr. **T137**, 014021 (2009).
[50] D. A. Lidar, I. L. Chuang, and K. B. Whaley, Decoherence-Free Subspaces for Quantum Computation, Phys. Rev. Lett. **81**, 2594 (1998).
[51] B. Kraus, H. P. Büchler, S. Diehl, A. Kantian, A. Micheli, and P. Zoller, Preparation of entangled states by quantum Markov processes, Phys. Rev. A **78**, 042307 (2008).
[52] T. A. Brun, Continuous measurements, quantum trajectories, and decoherent histories, Phys. Rev. A **61**, 042107 (2000).
[53] M. Schlosshauer, Quantum decoherence, Phys. Rep. **831**, 1 (2019).
[54] F. Motzoi, J. M. Gambetta, P. Rebentrost, and F. K. Wilhelm, Simple Pulses for Elimination of Leakage in Weakly Nonlinear Qubits, Phys. Rev. Lett. **103**, 110501 (2009).
[55] H. Paik, D. I. Schuster, L. S. Bishop, G. Kirchmair, G. Catelani, A. P. Sears, B. R. Johnson, M. J. Reagor, L. Frunzio, L. I. Glazman, S. M. Girvin, M. H. Devoret, and R. J. Schoelkopf, Observation of High Coherence in Josephson Junction Qubits Measured in a Three-Dimensional Circuit QED Architecture, Phys. Rev. Lett. **107**, 240501 (2011).
[56] E. L. Hahn, Spin echoes, Phys. Rev. **80**, 580 (1950).
[57] S. Sheldon, E. Magesan, J. M. Chow, and J. M. Gambetta, Procedure for systematically tuning up cross-talk in the cross-resonance gate, Phys. Rev. A **93**, 060302(R) (2016).
[58] J. A. Smolin, J. M. Gambetta, and G. Smith, Efficient Method for Computing the Maximum-Likelihood Quantum State from Measurements with Additive Gaussian Noise, Phys. Rev. Lett. **108**, 070502 (2012).
[59] J. J. Burnett, A. Bengtsson, M. Scigliuzzo, D. Niepce, M. Kudra, P. Delsing, and J. Bylander, Decoherence benchmarking of superconducting qubits, npj Quantum Inf. **5**, 54 (2019).
[60] J. Sun, X. Yuan, T. Tsunoda, V. Vedral, S. C. Benjamin, and S. Endo, Mitigating Realistic Noise in Practical Noisy Intermediate-Scale Quantum Devices, Phys. Rev. Appl. **15**, 034026 (2021).
[61] M. D. Shulman, O. E. Dial, S. P. Harvey, H. Bluhm, V. Umansky, and A. Yacoby, Demonstration of entanglement of electrostatically coupled singlet-triplet qubits, Science **336**, 202 (2012).
[62] J. M. Raimond, M. Brune, and S. Haroche, Reversible Decoherence of a Mesoscopic Superposition of Field States, Phys. Rev. Lett. **79**, 1964 (1997).
[63] M. Brune, E. Hagley, J. Dreyer, X. Maitre, A. Maali, C. Wunderlich, J. M. Raimond, and S. Haroche, Observing the Progressive Decoherence of the "Meter" in a Quantum Measurement, Phys. Rev. Lett. **77**, 4887 (1996).
[64] J. M. Chow, A. D. Córcoles, J. M. Gambetta, C. Rigetti, B. R. Johnson, J. A. Smolin, J. R. Rozen, G. A. Keefe, M. B. Rothwell, M. B. Ketchen, and M. Steffen, Simple All-Microwave Entangling Gate for Fixed-Frequency Superconducting Qubits, Phys. Rev. Lett. **107**, 080502 (2011).
[65] J. M. Gambetta, F. Motzoi, S. T. Merkel, and F. K. Wilhelm, Analytic control methods for high-fidelity unitary operations in a weakly nonlinear oscillator, Phys. Rev. A **83**, 012308 (2011).
[66] D. C. McKay, C. J. Wood, S. Sheldon, J. M. Chow, and J. M. Gambetta, Efficient Z gates for quantum computing, Phys. Rev. A **96**, 022330 (2017).
[67] E. Magesan and J. M. Gambetta, Effective Hamiltonian models of the cross-resonance gate, Phys. Rev. A **101**, 052308 (2020).
[68] N. Sundaresan, I. Lauer, E. Pritchett, E. Magesan, P. Jurcevic, and J. M. Gambetta, Reducing unitary and spectator errors in cross resonance with optimized rotary echoes, PRX Quantum **1**, 020318 (2020).